Rapid fragmentation of neuronal networks at the onset of propofol-induced unconsciousness

Laura D. Lewis[a,1], Veronica S. Weiner[a,1], Eran A. Mukamel[b,c], Jacob A. Donoghue[d,e], Emad N. Eskandar[f,g], Joseph R. Madsen[g,h], William S. Anderson[i], Leigh R. Hochberg[j,k,l], Sydney S. Cash[j,d], Emery N. Brown[a,e,m,n,o], and Patrick L. Purdon[m,n,2]

[a]Department of Brain and Cognitive Sciences, [e]Harvard–Massachusetts Institute of Technology Division of Health Sciences and Technology, and [o]Institute for Medical Engineering and Science, Massachusetts Institute of Technology, Cambridge, MA 02139; Departments of [m]Anesthesia, Critical Care and Pain Medicine, [j]Neurology, and [f]Neurosurgery, Massachusetts General Hospital, Boston, MA 02114; Departments of [n]Anesthesia, [d]Neurology, and [g]Surgery, Harvard Medical School, Boston, MA 02115; [b]Center for Brain Science, Harvard University, Cambridge, MA 02138; [c]Center for Theoretical Biological Physics, University of California at San Diego, La Jolla, CA 92093; [h]Department of Neurosurgery, Boston Children's Hospital, Boston, MA 02115; [i]Department of Neurosurgery, Johns Hopkins University School of Medicine, Baltimore, MD 21287; [k]Rehabilitation Research and Development Service, Department of Veterans Affairs, Providence, RI 02908; and [l]Institute for Brain Science, School of Engineering, Brown University, Providence, RI 02912

Edited* by Eve Marder, Brandeis University, Waltham, MA, and approved September 26, 2012 (received for review June 27, 2012)

The neurophysiological mechanisms by which anesthetic drugs cause loss of consciousness are poorly understood. Anesthetic actions at the molecular, cellular, and systems levels have been studied in detail at steady states of deep general anesthesia. However, little is known about how anesthetics alter neural activity during the transition into unconsciousness. We recorded simultaneous multiscale neural activity from human cortex, including ensembles of single neurons, local field potentials, and intracranial electrocorticograms, during induction of general anesthesia. We analyzed local and global neuronal network changes that occurred simultaneously with loss of consciousness. We show that propofol-induced unconsciousness occurs within seconds of the abrupt onset of a slow (<1 Hz) oscillation in the local field potential. This oscillation marks a state in which cortical neurons maintain local patterns of network activity, but this activity is fragmented across both time and space. Local (<4 mm) neuronal populations maintain the millisecond-scale connectivity patterns observed in the awake state, and spike rates fluctuate and can reach baseline levels. However, neuronal spiking occurs only within a limited slow oscillation-phase window and is silent otherwise, fragmenting the time course of neural activity. Unexpectedly, we found that these slow oscillations occur asynchronously across cortex, disrupting functional connectivity between cortical areas. We conclude that the onset of slow oscillations is a neural correlate of propofol-induced loss of consciousness, marking a shift to cortical dynamics in which local neuronal networks remain intact but become functionally isolated in time and space.

electrophysiology | single units | GABA | cortical networks

General anesthesia is a drug-induced reversible coma commonly initiated by administering a large dose of a fast-acting drug to induce unconsciousness within seconds (1). This state can be maintained as long as needed to execute surgical and many nonsurgical procedures. One of the most widely used anesthetics is propofol, an i.v. drug that enhances GABAergic inhibitory input to neurons (2–4), with effects in cortex, thalamus, brainstem, and spinal cord (5–7). Despite the understanding of propofol's molecular actions, it is not clear how these effects at molecular targets affect single neurons and larger-scale neural circuits to produce unconsciousness.

The effects on macroscopic dynamics are noticeable in the EEG, which contains several stereotyped patterns during maintenance of propofol general anesthesia. These patterns include increased delta (0.5–4 Hz) power (8, 9); increased gamma (25–40 Hz) power (9); an alpha (~10 Hz) rhythm (10–12) that is coherent across frontal cortex; and burst suppression, an alternation between bursts of high-voltage activity and periods of flat EEG lasting for several seconds (13, 14). In addition, slow oscillations (<1 Hz) have been well characterized in deeply anesthetized animals and are associated with an alternation of the neuronal membrane potential between UP (depolarized) and DOWN (hyperpolarized) states (8, 15).

Although these patterns are observed consistently, it is unclear how they are functionally related to unconsciousness under general anesthesia. Most studies have focused on a deep steady state of general anesthesia and have not used a systematic behavioral measure to track the transition into unconsciousness. This steady-state approach cannot distinguish between patterns that are characteristic of a deeply anesthetized brain and those that arise at the onset of unconsciousness. Unconsciousness can occur in tens of seconds (4), but many neurophysiological features continue to fluctuate for minutes after induction and are highly variable between different levels of general anesthesia (1, 16). Therefore, identifying the specific dynamics associated with loss of consciousness (LOC) requires an examination of the transition into unconsciousness, linking neurophysiology with behavioral measures.

In addition, the dynamic interactions between cortical areas that underlie these EEG oscillations are not well understood, because few studies have simultaneously recorded ensembles of single neurons and oscillatory dynamics from sites distributed across the brain. Consequently, how propofol acts on neural circuits to produce unconsciousness remains unclear. A leading hypothesis suggests that anesthetics disrupt cortical integration (17, 18). Identifying the mechanism by which this disruption might occur requires a better understanding of how the spatial and temporal organization of neural dynamics evolves during induction of unconsciousness.

To address this question, we investigated both neuronal and circuit-level dynamics in the human brain during induction of unconsciousness with propofol. We obtained simultaneous recordings of single units, local field potentials (LFPs), and intracranial electrocorticograms (ECoG) over up to 8 cm of cortex, enabling us

Author contributions: S.S.C., E.N.B., and P.L.P. designed the research; L.R.H. and S.S.C. established the microelectrode recordings; V.S.W., S.S.C., and P.L.P. collected the data; E.N.E., J.R.M., and W.S.A. performed the surgeries; L.D.L., E.A.M., J.A.D., S.S.C., E.N.B., and P.L.P. designed the data analysis; L.D.L., E.A.M., and J.A.D. performed the analysis; L.D.L. and P.L.P. wrote the paper.

Conflict of interest statement: E.N.B. and P.L.P have a patent pending on anesthesia monitoring.

*This Direct Submission article had a prearranged editor.

Freely available online through the PNAS open access option.

See Commentary on page 19876.

[1]L.D.L. and V.S.W. contributed equally to this work.

[2]To whom correspondence should be addressed. E-mail: patrickp@nmr.mgh.harvard.edu.

See Author Summary on page 19891 (volume 109, number 49).

This article contains supporting information online at www.pnas.org/lookup/suppl/doi:10.1073/pnas.1210907109/-/DCSupplemental.

to examine neural dynamics at multiple spatial scales with millisecond-scale temporal resolution. We used a behavioral task to identify within seconds the time at which patients became unresponsive to auditory stimuli, which we defined as LOC.

Our results reveal a set of neurophysiological features that accompany LOC that, together with previously reported effects (8, 9, 15), enable a multiscale account of this profound shift in brain state. We find that LOC is marked by the abrupt onset of slow oscillations (0.1–1 Hz) in the LFP. Power in the slow oscillation band rises sharply at LOC and maintains this increase throughout the post-LOC period. Neuronal spiking becomes coupled to the local slow oscillation within seconds of LOC: Spiking occurs only in short intervals of activity that are interspersed with suppression lasting hundreds of milliseconds, periodically interrupting information processing. These periods in which activity may occur are not simultaneous across the brain, implying that information transfer between distant (>2 cm) cortical networks is impaired. Cortical networks therefore are fragmented both temporally and spatially, disrupting both local and long-range communication. However, small-scale (<4 mm) functional connectivity measures remain similar to the conscious state, and neuronal spike rates can recover to baseline levels after LOC despite continued unresponsiveness. This result demonstrates that short periods of normal spike dynamics still can occur during unconsciousness. We conclude that the slow oscillation is a fundamental component of propofol-induced unconsciousness, marking a functional isolation of cortical regions while significant connectivity is preserved within local networks.

Results

We recorded single units (n = 198), LFPs, and ECoG in three patients undergoing intracranial monitoring for surgical treatment of epilepsy. Single units and LFPs were recorded from a 96-channel microelectrode array (19) implanted in temporal cortex for research purposes. We recorded throughout induction of general anesthesia by bolus administration of propofol before planned neurosurgery to remove the electrodes. Patients performed an auditory task requiring a button press in response to stimuli. All patients completely ceased responding to the task within 40 s of propofol administration and remained unresponsive for the remainder of the recording period, lasting 5–10 min after LOC. LOC was defined as the onset of this period of unresponsiveness to auditory stimuli. To acknowledge the fact that LOC could have occurred at any point between the last response and the failure to make the next response, LOC was defined as the interval beginning 1 s before the first missed stimulus up until the second missed stimulus (5 s total). We then compared spectra across all ECoG channels in the pre- and post-LOC periods. In agreement with previous scalp EEG studies of healthy subjects (9), we found that average spectra in the post-LOC period differed significantly from those in the pre-LOC period: Slow (0.1–1 Hz) and gamma (25–40 Hz) power increased in the unconscious state (Fig. S1). These results suggested that propofol acted as expected in these patients and did not reveal any gross disruption of GABA networks.

Spike Rates Are Highly Variable After LOC. To determine the relationship between changes in spike rate and LOC, we first examined the overall spike rate in a local network of cortical neurons. Consistent with propofol's enhancement of GABAergic signaling, widespread suppression of spiking was observed after LOC. In each patient, the spike rate across the population of units decreased significantly 0–30 s after LOC (Fig. 1 and Table S1; the range of values is the range across patients). Mean spike rates across all units reached a minimum 35–85 s after LOC, having decreased 81–92% from the baseline awake state. However, spike rates subsequently recovered over several minutes (Fig. 1*B*). At 4 min after LOC, the rate across the entire population of units varied widely, ranging from 33% of baseline in patient A to 117% of baseline in patient B. At this 4-min post-LOC period, individual units also displayed a wide range of spike rates, with some as high as or higher than baseline; only 35.2% of units still had spike rates significantly below baseline, 55.1% of units were not significantly different, and 9.7% of units had significantly increased spike rates. We conclude that propofol rapidly causes a nearly complete but transient suppression of cortical spiking, and after several minutes many individual neurons recover to baseline spike rates. The fluctuation in spike rates across time, which could have come about from changing propofol blood levels, demonstrates that brain state is dynamic after LOC. However, subjects remained unconscious throughout this period despite widely varying spike rates, suggesting that unconsciousness is not strictly associated with gross changes in spike rate.

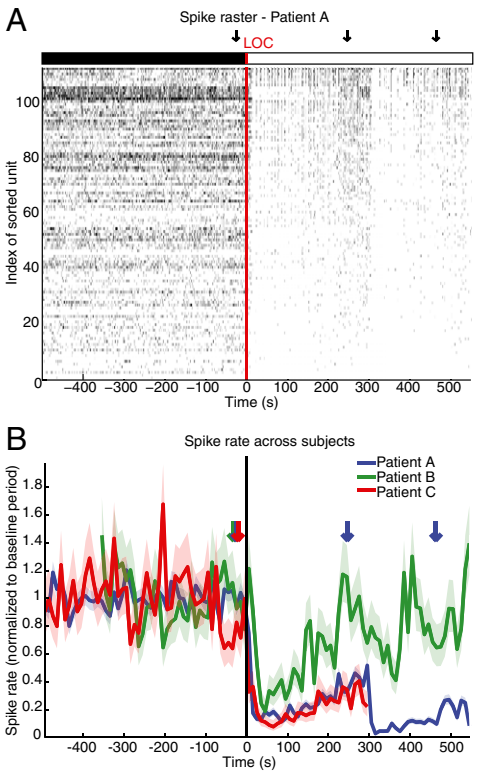

Fig. 1. Propofol induction of unconsciousness causes a sharp drop and slow recovery of spike rates. Arrows indicate approximate times of propofol administration (±20 s). (*A*) Sample spike raster from patient A. Units are sorted by post-LOC spike rate. Red line indicates time of LOC. A second drop in spike rate is visible after a second propofol bolus. (*B*) Bayesian state-space estimate of population spike rate by patient, locked to LOC (vertical black line). Population spike rate is normalized to pre-LOC period. Shaded region shows 95% confidence intervals. All spike rates drop within 0–30 s of LOC and then begin rising ~1 min after LOC (the second drop in patient A occurred after a second propofol bolus).

Spiking Activity Is Organized into Periods of Activity and Quiescence After LOC. Given that mean spike rates did not exhibit a fixed relationship with state of consciousness, we examined whether unconsciousness was associated instead with a change in the temporal structure of spiking. We observed that spiking activity across the population of units occurred in short periods of activity that were interrupted by periods of silence. To estimate conservatively the amount of time with no spike activity, we binned spikes from all units into 400-ms bins. We found that 63% of bins contained no spikes, significantly more than simulated neurons with a constant rate (33%, $P < 0.001$ for each patient, Pearson's χ^2 test). Therefore we concluded that cortical

networks can be highly active during unconsciousness, but this activity is concentrated in short periods that are followed by profound suppression.

Unconscious State Is Marked by a Rapid Increase and Stable Maintenance of Power in the Slow Oscillation Band. The slow oscillation is known to modulate neuronal spiking (8, 15), and therefore we examined the time course of its onset relative to LOC. Before LOC, power in the slow oscillation band (0.1–1 Hz) was stable (SD <7% in each patient before LOC). At LOC, power in the slow oscillation band increased abruptly by 35–70% (Fig. 2), and this power increase occurred within one 5-s window of LOC in all patients (Table S1). The slow oscillation power then persisted at this high level for the remainder of the recording, with 99.0% of the post-LOC time bins having higher slow oscillation power than occurred in any time bin during baseline (Fig. 2*A*). We therefore concluded that power in the slow oscillation band is modulated simultaneously with LOC and is preserved thereafter despite large fluctuations in spike rate.

We next examined other frequency bands to investigate whether the power change at LOC was specific to the slow oscillation band or whether other frequency bands showed a similar relationship. Although power in the >10 Hz range increased slowly after LOC, theta (3–8 Hz) power showed the opposite trend, decreasing 20–30% after LOC (Fig. 2*B* and Fig. S1). In addition, power in all these bands continued to undergo modulations for several minutes rather than maintaining a consistent change after LOC (Fig. S1), perhaps as the result of differences in propofol dosage during the maintenance phase. The stable increase in power at LOC therefore was specific to the slow oscillation band. These results demonstrated that both spike rates and many oscillatory features (gamma, alpha, theta) are highly variable after LOC. In contrast, slow oscillation power increased abruptly at LOC and remained elevated throughout the rest of the recording (Fig. 2*A*). Therefore we concluded that onset of power in the slow oscillation band is associated with the transition into unconsciousness, whereas other oscillatory features do not reach a steady state until minutes later and may reflect dynamic neural shifts at varying concentrations of propofol.

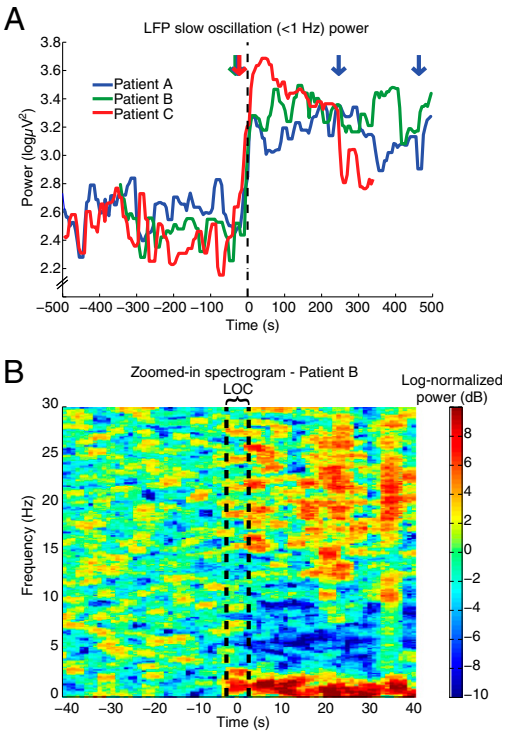

Fig. 2. The slow oscillation develops abruptly at LOC and is maintained thereafter. Dashed black line indicates LOC in both panels. (*A*) Slow oscillation (0.1–1 Hz) power in the LFP from a representative microelectrode across time, where time is computed relative to LOC. Slow oscillation power increases sharply at LOC in all patients and remains higher than baseline throughout the post-LOC period. (*B*) Zoomed-in spectrogram from a representative microelectrode in patient B, where power is normalized within each frequency band to the pre-LOC period. The abrupt and stable power increase after LOC is specific to the slow oscillation band.

Neuronal Spiking Becomes Phase-Coupled to the Slow Oscillation at LOC. Studies of deeply anesthetized animals have shown that neuronal spike activity is coupled to the phase of the slow oscillation (8, 15, 20). We examined whether this spike–phase relationship developed immediately at LOC and whether it was maintained consistently thereafter. In each patient, population spike activity after LOC was significantly phase-coupled to the LFP slow oscillation (0.1–1 Hz), with 46.6% of spikes from all units occurring near the trough of the slow oscillation, during a phase of 0 to $\pi/2$ (maximum spiking at a phase of $\pi/20$–$4\pi/20$). Phase-coupling developed within seconds of LOC (between −2.5 and 7.5 s; Table S1) and persisted throughout the ensuing changes in spike rate (Fig. 3 and Fig. S2). Spikes also were phase-coupled to the slow oscillation in the nearest ECoG channel but at a significantly different phase (maximum phase = 0 to $\pi/10$; $P < 0.001$, Kolmogorov–Smirnov test), suggesting that the LFP slow oscillation has a different relationship to spiking than the nearby, larger-scale ECoG recording. These results support the hypothesis that spikes become phase-coupled to the slow oscillation at LOC.

When examining individual units, most (67.2% of the 183 units with post-LOC spiking) were significantly phase-coupled to the LFP slow oscillation ($P < 0.05$, Pearson's χ^2 test). When this analysis was restricted to units with post-LOC spike rates over 0.1 Hz, 94.0% of units had significant phase coupling ($P < 0.05$, $n = 50$, Pearson's χ^2 test). Of the units without significant phase-coupling, 65.0% also showed peak spiking activity within a phase of 0 to $\pi/2$, demonstrating that most units had the same phase-coupling trend. These results demonstrated that after LOC nearly all spiking activity is tightly coupled to the slow oscillation phase and is suppressed for a large portion of the slow oscillation cycle. We refer to these periods of high spiking as "ON" states and the silent periods as "OFF" states to remain consistent with previous work using only extracellular recordings (21, 22). Because of the alternation of ON and OFF states, spike activity was limited to periods of a few hundred milliseconds, interrupted by periods of silence that also can last hundreds of milliseconds. Therefore we concluded that the slow oscillation marks a temporal fragmentation of cortical spiking that occurs at LOC.

Slow Oscillation Impairs Information Transfer Between Distant Cortical Regions. Given that post-LOC spiking is interrupted periodically within a cortical region, we investigated whether communication across distant areas also was affected. We examined slow dynamics across the grid of ECoG electrodes in the two patients (A and B) for whom we had at least 3 min of post-LOC ECoG data. Because spiking was strongly coupled to slow oscillation phase, we examined how this phase varied across the brain to infer the relative timing of neuronal activity in different cortical regions.

We quantified the phase relationships between different cortical regions using the phase-locking factor (PLF), which characterizes the phase offset between two oscillations over a period (23). The PLF magnitude ranges between 0 and 1 and quantifies the stability of the phase offset (1 reflects constant phase offset; 0 represents variable phase offset). The PLF angle indicates the average phase offset. We calculated the PLF between every pair of ECoG channels on the grid (8 × 4 or 8 × 8 cm, $n = 96$ total

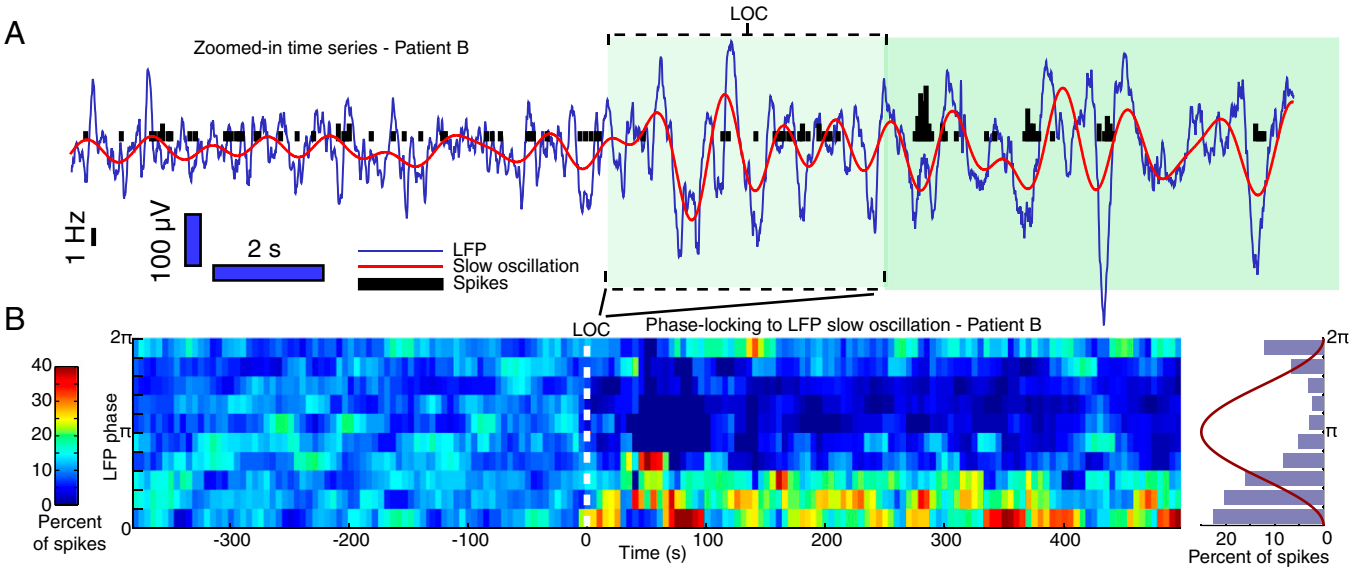

Fig. 3. Spikes become phase-coupled to the slow oscillation at LOC. Dashed line indicates LOC in both panels. (*A*) Sample LFP from a representative microelectrode in patient B. Filtered slow oscillation is overlaid in red, and the mean spike rate across all units is in black, showing onset of slow oscillation at LOC. The LOC period is shaded in light green and the post-LOC period in darker green. (*B*) (*Left*) Phase-coupling of all single units in patient B to their local LFP slow oscillation, where color indicates the percentage of spikes in a given phase bin. Plot demonstrates that phase-coupling begins at LOC. (*Right*) Red line shows a sinusoid to indicate slow oscillation phase. Histogram shows the phase distribution of all post-LOC spikes, which are coupled to the rising phase of the slow oscillation. See Fig. S2 for identical analysis of patients A and C.

electrodes) to determine the relationship between local and distant slow oscillations. We found that the PLF magnitude was conserved between the pre- and post-LOC states (correlation coefficient $R = 0.66$, patient A; $R = 0.88$, patient B; $P < 10^{-50}$ for each, t test), with a small but significant increase in PLF magnitude after LOC (mean increase = 0.02–0.07, $P < 0.01$, Wilcoxon signed rank test) (Fig. 4*A*). This result was consistent with previous findings that low-frequency correlations in neural activity are maintained after LOC (24, 25) and suggests that LOC is associated with only a slight shift in the strength of phase relationships between slow oscillations in different areas.

We next examined how the PLF varied with distance to determine whether slow oscillations in different cortical regions were at different phases. The PLF magnitude dropped significantly with distance ($R = -0.61$, patient A; $R = -0.82$, patient B; $P < 10^{-6}$ for each) (Figs. 4B and 5C and Fig. S3), demonstrating that the phase offsets between distant slow oscillations were variable. We also examined the mean phase offsets (PLF angle). Mean phase offsets between distant channels varied across a wide range, spanning 0 to π (Fig. 4*C* and Fig. S3). Because a phase offset of just π/4 corresponds to a lag of ∼250 ms, slow oscillations in distant ECoG channels had substantial timing differences. These results demonstrated that distant slow oscillations often were at different phases than the local oscillation, and these phase differences were not stable across time.

To examine how these phase offsets would affect neuronal activity, we examined the phase relationship between local spiking and slow oscillations measured across the ECoG grid. We measured spike phase-coupling as a modulation index (MI) quantifying the Kullback–Liebler divergence, in bits, between the observed phase distribution and a uniform distribution (*Methods*). A large MI indicates a strong relationship between local spiking and ECoG phase, whereas an MI of zero indicates no relationship. In the pre-LOC period, MI values were consistently small across all ECoG channels (MI range: 0.001–0.04 bits) (Fig. 5*D*), demonstrating that slow oscillation phase was not associated with strong suppression of spiking in the pre-LOC period. After LOC, the MI was significantly more variable across channels (range: 0.006–0.62 bits, $P < 0.01$ in each patient, Levene's test). Spikes were strongly phase-coupled to the slow oscillation in the nearest ECoG channel, and this relationship declined significantly with distance ($R = -0.40$, patient A; $R = -0.68$, Patient B; $P < 0.001$ in each patient) (Fig. 5 *B* and *D* and Fig. S4).

Taken together, our analysis of phase–phase and spike–phase coupling show that the post-LOC state is characterized by periodic and profound suppression of spiking coupled to the local slow oscillation phase and that this phase is not consistent across cortex. Given the strong relationship between phase and ON/OFF periods, this result suggests that, after LOC, ON periods in distant (>2 cm) cortical regions occur at different times (Fig. 5*E*, *Right*). In contrast, low-frequency oscillations in the pre-LOC state are not associated with strong suppression of spiking, so neurons are able to fire at any phase of local or distant slow oscillations despite the presence of phase offsets (Fig. 5*E*, *Left*). The combination of phase offsets and strong phase-coupling of spikes that occurs at LOC therefore is expected to disrupt communication between distant cortical areas, because one cortical area frequently will be profoundly suppressed when another area is active.

Although spikes were not strongly phase-coupled to distant slow oscillations during the post-LOC period, several electrodes located more than 3 cm from the spike recording site showed a statistically significant relationship (Fig. S5). In these cases, phase-coupling was weak, and the phase of maximal spiking was shifted, consistent with our conclusion that distant cortical regions are unlikely to have simultaneous ON periods. However, this finding raises the possibility that, despite the asynchrony of slow oscillations across the brain, there might still be a link between slow oscillations in distant cortical regions. Given the observed phase offsets (which ranged up to π), such coupling would occur frequently over hundreds of milliseconds and would not reflect precisely timed inputs and interactions. Overall, these analyses support the conclusion that distant cortical regions frequently were at a suppressed phase of the slow oscillation when the local

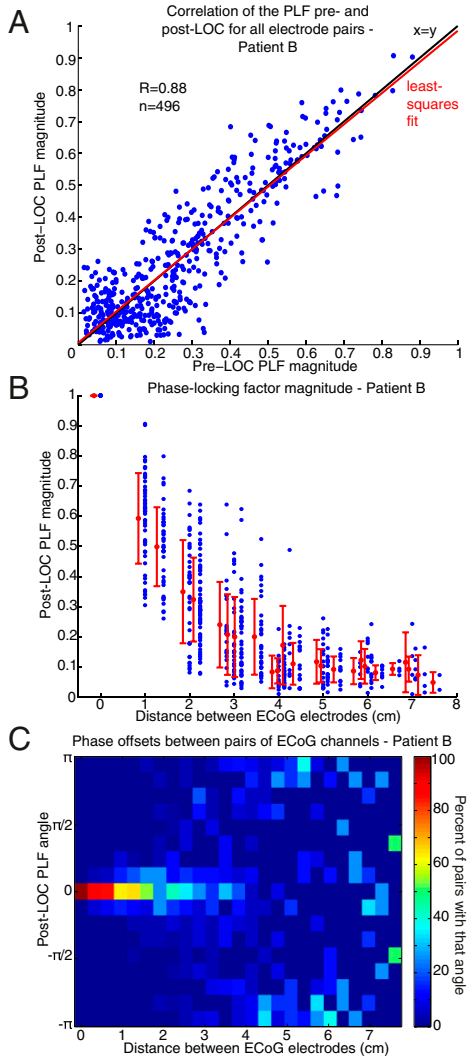

Fig. 4. Slow oscillations in distant ECoG channels have variable phase offsets. The PLF characterizes the stability of the phase offset between two oscillations over a period, selected as either pre- or post-LOC. The PLF magnitude ranges between 0 and 1, where 1 reflects constant phase offset, and 0 represents variable phase offset. The PLF angle indicates the average phase offset. (*A*) PLF magnitude between each pair of ECoG electrodes, with pre-LOC PLF on the *x*-axis and post-LOC PLF on the *y*-axis. Pre- and post-LOC PLF magnitude are highly correlated. The red line marks the line of best fit to the data. (*B*) PLF magnitude during the post-LOC recording, plotted according to the distance between the electrodes in each pair. The PLF magnitude decreases significantly with distance, reflecting higher variability in phase offsets between distant ECoG electrodes. Red lines show mean (± SD) PLF magnitude over all electrode pairs at that distance. (*C*) 2D histogram of the PLF angle between all ECoG pairs after LOC, showing that the mean phase offset is more variable between distant channels, with values as large as π, than between nearby channels.

network was active. Therefore activity within a cortical area was isolated, impairing communication between distant regions.

Local Network Structure Is Preserved After LOC. Having observed interruptions in local activity and disruption of long-range communication, we examined whether connectivity within the local cortical network also was impaired. We fit a generalized linear model (GLM) to spike activity from the ensemble of units to test whether spiking could be predicted by the slow oscillation phase alone or whether the history of local network activity also contributed (26). We used the Bayesian Information Criterion (27) to select the number of covariates to include in the model. In each patient, we found that this model included >30 ms of population spike history (Fig. 6*A* and Fig. S6). Ensemble spike history therefore predicted future spiking, demonstrating that, although cortical activity was limited to brief ON periods, interunit structure existed within these periods. This pattern resembled the pre-LOC state, in which recent spike history (0–48 ms) was predictive of future spikes and more distant spike history contributed less (Fig. S7). This result suggests that, after LOC, cortical activity is not reduced to disordered spiking during ON periods. Instead, significant structure is maintained between nearby neurons during their brief periods of activity.

Structure between single units was reflected further in a peak in the cross-intensity function between several pairs of units, demonstrating millisecond-scale synchronization of spike activity (Fig. 6 *B* and *C*). To examine whether pairwise synchronization persisted after LOC, we analyzed the cross-correlation between the 15 units with the highest spike rates in patient A. Of the 103 pairs (excluding pairs recorded on the same electrode), 21 were significantly correlated before LOC ($P < 0.05$, exact Poisson test relative to baseline from shuffled spikes, Bonferroni correction for multiple comparisons). After LOC, 71.4% of these pairs remained significantly correlated. In contrast, a significantly smaller number (only 18.3%) of pairs that were not correlated before LOC became correlated after LOC ($P < 10^{-5}$, Fisher's exact test). This result demonstrated that pairs of units tended to retain the same correlation structure after LOC that they had before LOC, whether it was the presence or absence of a correlation. Taken together, both the GLM and paired correlation results show that significant interunit connectivity is maintained within post-LOC ON periods. This result suggests that the dominant change after LOC is the isolation of cortical networks, whereas aspects of local network structure may remain unaltered.

Spiking Activity Is Associated with Modulations in Slow Oscillation Shape and Higher Frequency Power. The mechanisms underlying the slow oscillation are debated (20, 28–31). Therefore, we examined the relationship between spike activity and slow oscillation shape in greater detail. We calculated an average LFP triggered at the beginning of ON periods. The triggered average demonstrated that ON periods begin at the minimum of the LFP slow oscillation (Fig. 7 *B* and *C*). In addition, the LFP slow oscillation was asymmetric (Fig. 7*C*), with a higher peak after spiking than before spiking (mean difference = 40.7 μV, $P < 10^{-5}$, $P < 0.005$ for each patient, *t* test). We tested whether this asymmetric shape occurred on all cycles of the slow oscillation or was specific to cycles with high spike activity. We compared cycles of the LFP slow oscillation that contained spikes with cycles that did not, matching the amplitudes of the slow oscillation minimum. Cycles that were not associated with spikes were symmetric (mean difference = 0.3 μV, $P > 0.9$, *t* test), whereas those that were associated with many spikes produced a higher peak after spiking (mean difference = 32.2 μV, $P < 0.001$, $P < 0.05$ for each patient, *t* test) (Fig. 7*D*). This asymmetry did not extend to the nearby ECoG recording (Fig. S8), suggesting that the relationship between spike activity and slow oscillation shape is a highly local effect limited to less than 1 cm (i.e., the spacing in the ECoG grid). These results demonstrated that high spike rates are associated with an increased slow oscillation peak in the LFP, potentially reflecting enhanced suppression after spike activity.

Because low gamma (25–50 Hz) power also increased after LOC (Fig. S1 and Table S1), we examined its relationship to spike activity as well. ON periods were associated with significantly increased broadband (<50 Hz) power in the LFP and ECoG ($P < 0.05$, F-test, Bonferroni correction for multiple comparisons across frequencies) (Fig. 7*A* and Fig. S8). LFP power in alpha, beta, and gamma bands was significantly higher in slow oscillation cycles with high spike activity than in cycles with low spike activity

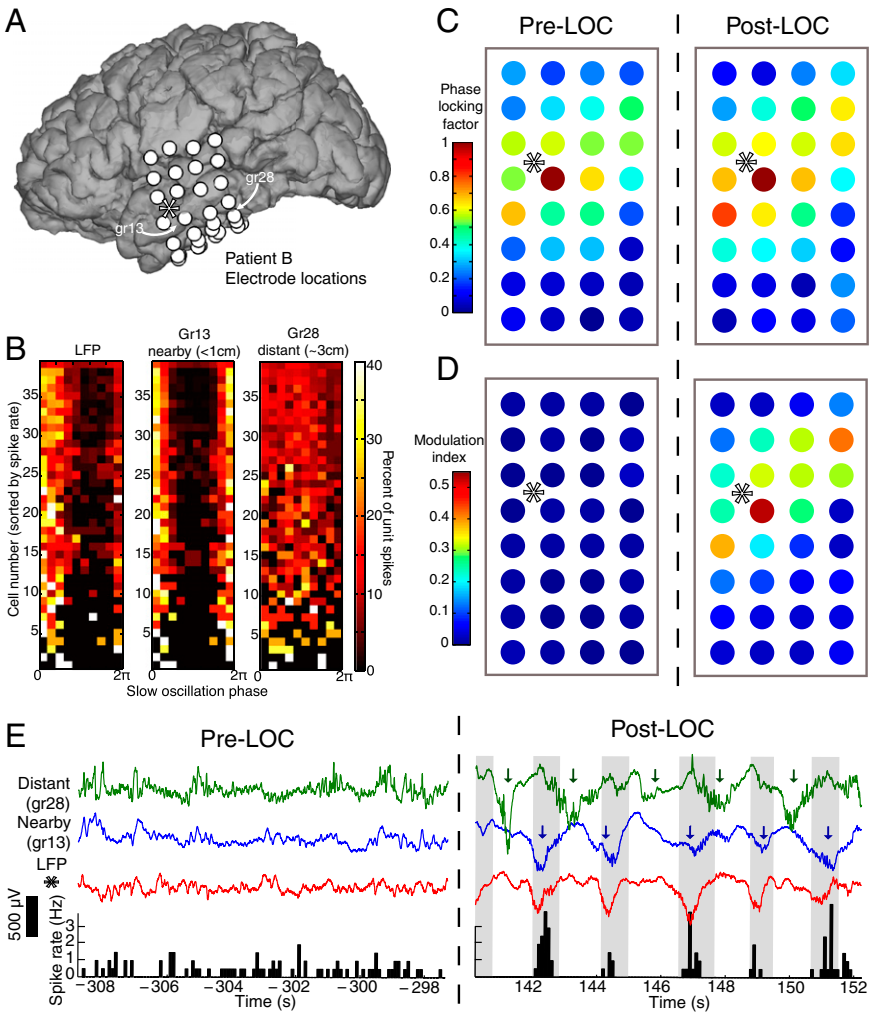

Fig. 5. After LOC, slow oscillations are asynchronous across cortex and are associated with ON/OFF states; therefore, distant cortical areas frequently are at a suppressed phase during local ON periods. (*A*) Position of ECoG and microelectrode recordings in patient B. Each white circle marks the location of an ECoG electrode, and the microelectrode where spikes were recorded is marked with a star. (*B*) Phase histograms for every single unit in patient B. Each panel displays the spike coupling to phase in a different recording site. Units are arranged by post-LOC spike rate with the highest rate at top of plot, and the same phase-coupling trend is visible across all units to the phase of the LFP and nearby ECoG (gr13). In contrast, the slow oscillation in the distant ECoG channel (gr28) does not have the same phase relationship to local spiking. (*C*) Magnitude of the PLF between every ECoG electrode relative to the ECoG closest to the spike recordings (gr13). The PLF drops with distance in both the pre- and post-LOC states, showing that distant areas have variable phase offsets relative to the local recording. (*D*) MI quantifying the strength of the spike–phase relationship. The MI is consistently low in the pre-LOC state, demonstrating the absence of a strong spike–phase relationship. After LOC, the MI is high only in local ECoG recordings, demonstrating that spikes are strongly phase-coupled to local slow oscillations and that this relationship weakens with distance. (*E*) Traces from a nearby ECoG (blue), distant ECoG (green), representative LFP channel (red), and mean spike rate across all units (black). Arrows mark the times that the ECoG slow oscillation is at phase zero (when local spike rates are expected to be high; see Fig. 3). Gray shading marks the times at which the LFP slow oscillation phase is between $-\pi/4$ and $3\pi/4$, when most spiking occurs. Plots show that, after LOC, local spikes occur in ON periods that typically overlap with the zero phase in the nearby ECoG channel but frequently do not overlap with the zero phase in the distant ECoG channel.

($P < 0.05$, F-test, Bonferroni correction for multiple comparisons across frequencies) (Fig. 7*E*). These results showed that, in addition to the slow changes in gamma power occurring over minutes (Fig. S1), gamma power also fluctuated at the timescale of the slow oscillation (0.1–1 Hz) and was higher during ON periods. Therefore we concluded that after LOC power in the low gamma range is associated with high local spike rates. This result suggested that the gradual increase in gamma power after LOC may be related to the post-LOC fluctuations in spike rate rather than reflecting dynamics induced specifically at LOC.

Discussion

In summary, we found that rapid induction of unconsciousness using propofol causes the human brain to undergo an abrupt change in network dynamics, tipping into a new state in which neuronal activity is coupled to slow oscillations in the LFPs. Neural dynamics can be highly variable during the unconscious period, as spike rates and most oscillatory patterns continue to fluctuate for minutes after LOC (Fig. 1 and Fig. S1). The slow oscillation has a markedly different pattern: It develops simultaneously with LOC and maintains this increase thereafter (Figs. 2 and 3). Spiking activity is constrained to brief time periods coupled to the phase of the slow oscillation (Figs. 3 and 5), interrupting information processing within a cortical area. Moreover, these brief activity periods are phase-shifted across cortex (Figs. 4 and 5), limiting activity spatially, because different cortical areas are likely to be active at different times. However, functional connectivity within the local network is preserved

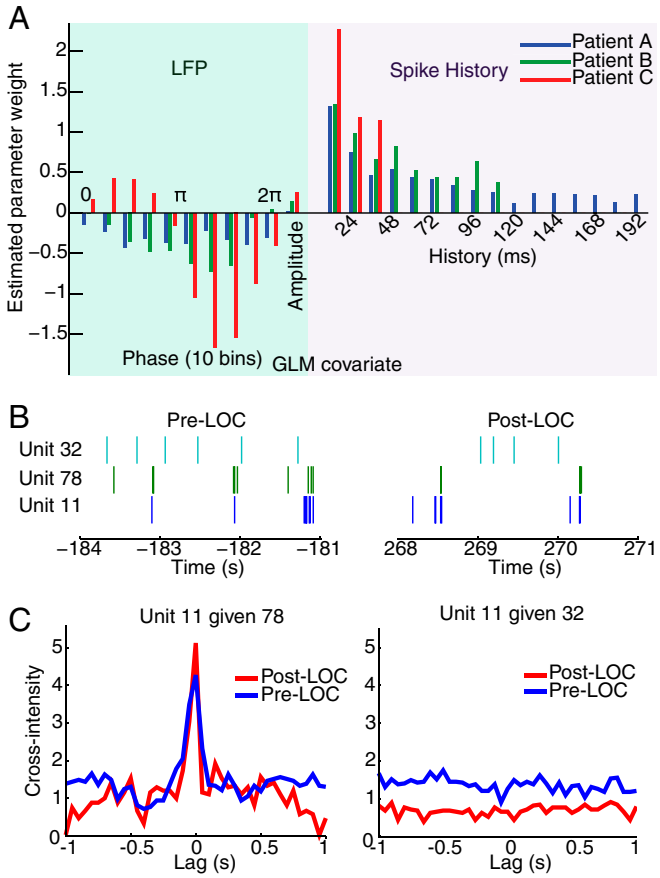

Fig. 6. Spikes occur in brief ON periods that maintain interunit structure. (*A*) Parameter estimates from the best GLM model for population spiking after LOC. For each patient, the best model includes information from both LFP phase and recent population spike history. (*B*) Time-series example. Units 11 and 78 spike together; unit 32 has a similar spike rate but does not. These units preserve the same correlation structure after LOC that they had before LOC. (*C*) Example of cross-intensity functions [square-root estimate (51)] before and after LOC, showing that the pre-LOC interunit structure persists after LOC.

(Fig. 6). These results suggest that the slow oscillation prevents both sustained information processing within an area and communication between distant cortical areas. General anesthetics have been proposed to cause unconsciousness by disrupting cortical integration (17, 18). Our results are consistent with this hypothesis and demonstrate that, in the case of propofol, spatiotemporal slow oscillation dynamics may mediate the breakdown of communication by isolating local cortical networks.

Slow Oscillations and Functional Connectivity. The slow dynamics reported here also may underlie the observation that gamma coherence decreases after propofol-induced LOC, particularly across distant cortical regions (18, 32). We found that spiking activity is strongly associated with gamma power (Fig. 7), and spiking is unlikely to occur simultaneously in distant cortical regions because of the asynchronicity of slow oscillations across the brain (Fig. 4). Slow oscillations therefore may impair coupling of gamma oscillations between cortical areas, and this effect could produce gamma oscillations that are not coherent over long distances.

Low-frequency spatial correlations in fMRI (25) and ECoG (24), sometimes used to assess functional connectivity, have been found to remain invariant after LOC under propofol. Our analysis of the PLF magnitude, which has a similar spatial distribution before and after LOC (Fig. 4*A*), corroborates this observation. Our studies show that although the low-frequency spatial relationships remain similar before and after LOC, the functional properties of low-frequency oscillations change at LOC, grouping spiking into brief ON states that are disjoint across space.

Potential Circuit Mechanisms Underlying the Slow Oscillation. The mechanisms underlying the slow oscillation are unclear. One hypothesis is that the slow oscillation is cortically generated (20, 28, 29), but others suggest that it results from an interaction between cortex, thalamus, and thalamic reticular nucleus (30, 31). The relationship identified here between spike activity and slow oscillation shape suggests that cortical spiking may have a causal role in the slow oscillation. Spikes predict a high-amplitude peak in the LFP slow oscillation (Fig. 7*D*), but this effect does not extend to the ECoG recordings, which integrate activity from a larger population of neurons. The highly local nature of this effect suggests that cortical spiking may affect the local slow oscillation directly. One possible mechanism is that pyramidal neuron spiking during ON periods excites GABAergic interneurons, whose inhibitory actions are enhanced by propofol, driving the local network into a more hyperpolarized state. Another possibility is that spike activity may drive disfacilitation of cortical neurons, a mechanism that has been demonstrated in slow-wave sleep (33). These effects could be consistent with either the cortical or corticothalamic hypothesis.

Slow Oscillations in General Anesthesia and in Sleep. The slow oscillation during propofol-induced unconsciousness shares several features with slow waves during sleep: In both states, spike activity is coupled to a local slow oscillation that is not synchronous across the brain (21). The asynchronicity observed here (Figs. 4 and 5E) contrasts with previous observations in anesthetized animals (34) and is most likely caused by the increased spatial sampling provided by the 8-cm grid of intracranial electrodes. In addition, the preservation of pre-LOC neuronal network properties after LOC (Fig. 6) is consistent with the hypothesis that cortical UP states during sleep have dynamics similar to the waking state (35).

However, the patterns observed under propofol also show striking differences from patterns during sleep. The onset of the slow oscillation during induction of general anesthesia was abrupt (Figs. 2 and 3), accompanying rapid LOC caused by the bolus administration of propofol. Because general anesthesia typically is induced with a bolus of propofol, this abrupt transition into the slow oscillation is likely to occur in the majority of clinical patients when they lose consciousness during general anesthesia. During sleep, the slow oscillation develops over minutes, consistent with the gradual nature of the transition into sleep (36, 37). In both cases, slow oscillation dynamics temporally track LOC, further supporting the proposal that the slow oscillation represents a breakdown of cortical communication.

In addition, we found that periods of spike activity were brief (Fig. 5*E*), whereas sleep is characterized by persistent spiking with brief periods of suppression during slow-wave events (21, 38–40). This observation was corroborated recently in a study of sleeping and anesthetized cats (41). A difference in the ratio of UP and DOWN states could provide one explanation for why propofol creates a more profound disruption of consciousness than sleep: There is less temporal overlap in neuronal spiking between different cortical regions, more reliably preventing the organization of large-scale population activity. Furthermore, recent findings that isolated OFF states in sleep-deprived rodents are associated with behavioral impairment (42) are consistent with the hypothesis that the spatial and temporal properties of OFF states affect cortical function.

Potential Role of Slow Oscillations in Unconsciousness. Our results show that the slow oscillation appears abruptly at the onset of propofol-induced LOC. In addition, we demonstrate that the slow oscillation marks a state in which neuronal networks are

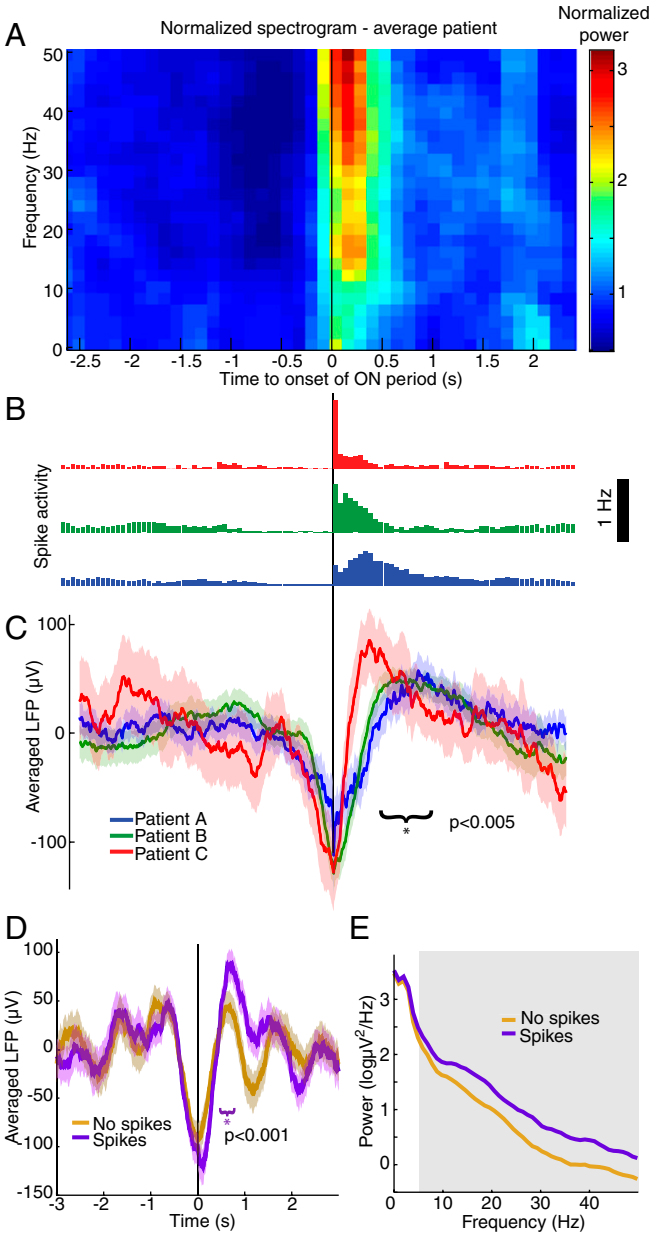

Fig. 7. Spike activity is associated with modulations in slow oscillation morphology and gamma power. (*A*) LFP spectrogram triggered at onset of ON periods (black line). Power is normalized within each band and log-transformed. (*B*) Population spike histograms for each patient, demonstrating spike activity locked to ON period detection times. (*C*) LFP average time-series triggered at ON period onset times, showing an increased LFP peak after spike activity compared with before spike activity. Shaded region indicates approximate 95% confidence intervals. The slow oscillation peak is significantly higher after spiking than before spiking. (*D*) LFP triggered at troughs of the slow oscillation. Purple trials are cycles of the slow oscillation associated with many spikes, and brown trials are cycles that were not associated with any detected spikes (n = 153 cycles per condition, drawn from all three patients). Only trials associated with high spike rates show an asymmetric LFP peak. The shaded region indicates approximate 95% confidence intervals. (*E*) Power spectra of LFP time-series triggered at the trough of the slow oscillation. Gray region indicates significant difference in >10 Hz power during trials with high spike rates.

fragmented, impairing both local and long-range communication. However, the scope of this study, performed in human subjects, does not allow us to test explicitly the causal role of the slow oscillation in unconsciousness. Furthermore, this experiment defines LOC as loss of voluntary response but cannot disambiguate whether the ability to respond may be suppressed before LOC. Given the slow oscillation's association with prolonged and asynchronous periods of nearly complete suppression of neuronal activity, it seems unlikely that it is compatible with conscious processing. However, other possible mechanisms for propofol-induced unconsciousness include coherent frontal alpha rhythms that limit thalamocortical function (11, 12, 43). Future work in animal models could test whether the slow oscillation is sufficient to produce unconsciousness.

Generalizability of Propofol-Induced Slow Oscillations. A limitation of this study is that we enrolled patients with epilepsy, and it is possible that their cortical networks differed because of seizure foci or medication history. However, several factors support the hypothesis that these results generalize to the healthy brain. First, the microelectrodes were located at least 2 cm from the seizure focus in each patient, and histology did not reveal any disruption of the local network, suggesting that the LFPs and single units were recorded from healthy cortex. Second, the overall effects of propofol were highly consistent with those observed in healthy subjects: Unconsciousness was associated with increased slow oscillation power and increased gamma power, in strong agreement with previous studies (9). These results suggest that propofol acted typically in these patients' brains. Finally, we report statistics for each individual patient and show that the timing of the slow oscillation onset and its relationship to spiking were replicated across patients despite their individual clinical profiles. Because epilepsy is a heterogeneous disease with different cortical origins, the high consistency of these results suggests that the effects reported here are not caused by the presence of epilepsy. These three observations suggest that our results are not a product of an epileptic brain but rather reflect a true neural correlate of LOC that is likely to generalize to the healthy brain. Future studies in patients with pathologies other than epilepsy could address this issue further.

Role of Slow Oscillations in Other Brain States. Other anesthetic drugs, such as ketamine and dexmedetomidine, operate through molecular and neural circuit mechanisms different from those of propofol (4). The study presented here provides a framework for studying these other drugs further and identifying how they influence neural dynamics to produce altered states of arousal. In addition, further work will be needed to explore how these findings may relate to other conditions, because slow-wave activity is a common feature in conditions such as coma (44) and complex-partial seizures (45), and those slow waves share some characteristics with the slow oscillations studied here. Although a unitary mechanism for unconsciousness under general anesthesia is technically possible, it is more likely that a variety of mechanisms exist that can produce unconsciousness (2). We have shown here that the slow oscillation is a fundamental component of propofol-induced unconsciousness, marking an impairment of cortical integration at both the local and global scale.

Methods

Data Collection. Three patients with epilepsy intractable to medication were implanted with intracranial subdural electrocorticography electrodes for standard clinical monitoring (AdTech). Informed consent was obtained from all patients in accordance with the Partners Human Research Committee. ECoG electrode placement was determined solely by clinical criteria, and the electrodes were located in temporal, frontal, and parietal cortices. Individual ECoG electrodes within a grid were spaced 1 cm apart. In addition, a 96-channel NeuroPort microelectrode array with 1.0-mm–long electrodes (BlackRock Microsystems) was implanted into the superior (patient B) or middle (patients A and C) temporal gyrus to record LFPs and ensembles of single units for research purposes. In each patient, the Neuroport array was located at least 2 cm from the seizure focus. There was no evidence of

disruption in local network structure based on the firing properties of the neurons or the postresection histological examination of the area around the array. All recordings were collected at the beginning of surgery to explant the electrodes. Anesthesia was administered as a bolus dose of propofol according to standard clinical protocol. All propofol doses were based on the anesthesiologist's clinical judgment rather than the research study considerations. Patient A received three boluses (130 mg, 50 mg, and 20 mg), patient B received one bolus (200 mg), and patient C received one (150 mg). After induction, patients were transferred to a continuous i.v. infusion of propofol to maintain anesthetic levels. Throughout the induction period, patients responded to auditory stimuli (prerecorded words and the patient's name) with a button press, and stimuli were presented every 4 s to obtain precision for LOC time on the order of seconds. LOC time was defined as the period from −1 to 4 s surrounding the first stimulus after the patient completely ceased responding. Spike sorting was carried out according to standard procedures (46) with Offline Sorter (Plexon) and produced 198 single units for further analysis. LFPs were referenced to a wire distant from the microelectrode array and were collected with hardware filters bandpassing between 0.3–7,500 Hz with a sampling rate of 30 kHz. LFPs then were low-pass–filtered at 100 Hz and resampled to 250 Hz. For display, raw time-series were low-pass–filtered with a finite-impulse response filter with 4,464 coefficients, achieving unit gain between 0 and 40 Hz and attenuation of more than −300 dB above 42 Hz. ECoG recordings were collected with a sampling rate of either 250 Hz (patients B and C) or 2,000 Hz (patient A), in which case it was low-pass–filtered at 100 Hz and resampled to 250 Hz. ECoG recordings were referenced to an intracranial reference strip channel when available (patient A) and otherwise to an average reference. In patients A and B, ECoG recordings were collected throughout. In patient C, the microelectrode recordings were collected throughout, but the ECoG recording ended ∼100 s after LOC; therefore the significance of slow oscillation phase-coupling could not be assessed in ECoG channels, because the spike rate was nearly zero during this time. Two ECoG grid channels were rejected in patient A because of large artifacts. All data were exported to Matlab (Mathworks) for analysis with custom software.

Spike Rate Analysis. Spike rates and confidence intervals were computed with Bayesian state-space estimation (47). To minimize any error caused by unstable recordings, the spike rate analysis excluded units that were not confidently detected throughout the entire baseline period (8.1%). The computed spike-rate effects were similar when these units were included. Periods of silence were compared with a simulated Poisson distribution of equal rate over each 10-s period, and significance was assessed for each patient with a χ^2 test relative to that distribution.

Spectral Analysis. Spectrograms were calculated with multitaper methods using the Chronux toolbox (http://chronux.org/; for bandwidth settings, see *SI Methods*). Power changes after LOC were computed as the percent change in the period 30–60 s after LOC relative to the period 30–60 s before LOC. Ranges in the text reflect ranges across patients. The slow oscillation was extracted by applying a symmetric finite impulse-response bandpass filter with 4,464 coefficients, achieving unit gain from 0.1–1 Hz and attenuation of more than −50 dB from 0–0.85 and 1.15–125 Hz. Because of hardware filter settings with a high pass at 0.3 Hz, the power contribution below 0.3 Hz was minimized. Phase was extracted with a Hilbert transform. Statistical testing of triggered spectrograms was done by taking a ratio of each χ^2 distribution, and significance was calculated as an F-test with a Bonferroni correction for multiple comparisons across frequencies. For comparing spectra during and before an ON period, power spectra from 250 ms after ON period onset were compared with spectra from 250 ms before the ON period onset. Averaged LFP waveforms were compared by preselecting a time period and performing a *t* test on the mean amplitude values within that interval. When comparing the waveform height before and after spiking, a *t* test was performed comparing the mean amplitude in the time window from −750 to 500 ms and in the time window from 500–750 ms locked to ON period onset or slow oscillation minimum.

Phase Modulation. Significance for single-unit phase-coupling was computed with a χ^2 test on the binned phase distribution. The analysis was performed a second time on only cells with spike rates above 0.1 Hz, ensuring that there were at least five expected spikes per phase bin. Strength of phase modulation was computed as an MI (48) adapted to quantify the Kullback–Liebler divergence of the phase histogram from the uniform distribution, measured in bits. Spike phase was split into a phase histogram (p) of 10 bins, and MI was computed as $\sum_{i=1}^{10} p_i \log_2 p_i + \log_2 10$. We also computed the χ^2 statistic as an alternative measure, yielding similar results. MI significance for each ECoG channel was calculated by shuffling the entire spike train randomly between 2 and 10 s and calculating a shuffled MI over 2,000 random shifts. The empirical MI then was compared with the shuffled MI with a significance level of 0.05 and a Bonferroni correction for multiple comparisons across channels. For LFP phase analysis, each single unit was compared with its local LFP channel. The time-varying phase modulation was computed with a window of 20 s sliding every 5 s. To assess the phase of maximal spiking relative to the ECoG slow oscillations, the phase of spiking was divided into 20 bins, and then the mode of the phase histogram was reported.

Timing of Spike Rate and Spectral Power Changes Relative to LOC. We tested spike rates and spectral power to determine the first time bin in which these features differed significantly from the baseline period before propofol administration. We compared every time point, starting 30 s before LOC, with a baseline of spike rates or spectral features from the 3-min baseline period immediately preceding it. To assess spike rate significance, we used a Bayesian hierarchical analysis in which each postbaseline time point was compared with samples drawn from the Gaussian distribution of the baseline period and tested for a significant difference. This baseline sampling distribution was computed with the same state-space algorithm used to calculate spike rates (47). To determine the time at which power at a given frequency differed significantly, we used an analogous method but replaced the Gaussian sampling distribution with a χ^2 distribution, which is the appropriate distribution for power measures. The time bin in Table S1 lists the earliest point at which the value had a 95% probability of being higher than the baseline period. We could not construct a similar sampling test for the MI because its distribution is not known, so we did not resample the baseline and instead reported the time at which MI became higher than the mean of the baseline period plus two SDs. For all these measures, 5-s nonoverlapping bins were used to identify the time at which changes occurred relative to LOC, which is the period from −2.5 to 2.5 s.

PLF. The PLF was computed to obtain a time-varying measure of phase offsets between slow oscillations. The phase of the slow oscillation was extracted as described in *Spectral Analysis*. For each time point, we then computed $z(t) = \exp\{-i^*[\varphi(t) - \varphi(t)]\}$ where $\varphi_A(t)$ is the phase of one ECoG slow oscillation at each time point and $\varphi_B(t)$ is the phase of another ECoG slow oscillation. The PLF then was calculated as the mean of $z(t)$ across the pre-LOC periods and across the post-LOC period. To assess the variability of phase offsets, we calculated the magnitude of the PLF. The distribution of PLF magnitude was assessed by plotting the mean and SD of the PLF magnitude across each pair of ECoG channels separated by a given distance (the distance between channels computed geometrically across the grid). To determine the mean value of the phase offset across time, we calculated the angle of the PLF. We then plotted the distribution of mean phase offsets across all pairs of channels separated by a given distance, by taking a 2D histogram of PLF angle values for all electrode pairs. Accompanying reconstructed brain showed individually localized electrode positions (49).

GLM Fitting. A GLM was fit to ensemble spiking using custom software that performed regression with Truncated Regularized Iteratively Reweighted Least Squares (TR-IRLS) (26, 50) and using the Bayesian Information Criterion to select the best model. Using the Akaike's Information Criterion also yielded a significant contribution of spike history. The GLM was constructed to predict ensemble spiking, which was defined as a series of 12-ms bins that contained a 1 if any spikes from any units occurred in that period and a 0 otherwise. Ten covariates were used to represent the range of possible LFP phase values. Amplitude was normalized to range between 0 and 1. Because individual unit spike rates are low, the history-dependent terms in this model predominately reflect interactions between units. The version presented is with 12-ms bins of spike history; similar results were obtained when using 4- or 8-ms bins. We excluded the minute surrounding LOC to ensure that any correlation between pre-LOC and post-LOC analyses did not result from bias from adjacent recordings during the LOC transition. For detailed equations, see *SI Methods*.

Single-Unit Correlations. Single units with high post-LOC spike rates were selected for correlation analysis to ensure sufficient spikes to assess the significance of their correlations. The minute surrounding LOC was excluded to reduce bias that could result from comparing adjacent recordings. Correlations between single units were computed relative to a shuffled baseline, to examine fine time-scale synchronization beyond the changes in population spike rate induced by the slow oscillation. Spike times were randomly shuffled 200 times, between 50 and 500 ms, to obtain a baseline of correlated spike rate without millisecond-level timing information. Paired correlations then were tested for significance between −100 and 100 ms, with $P < 0.05$ using a Bonferroni correction for multiple comparisons across lags. Correlations

were judged significant if they had a $P < 0.05$ departure from the Poisson distribution of spike occurrence predicted by the shuffled baseline. The relationship between pairs of single units was visualized with the square root of the estimate of the cross-intensity function (51). Fisher's exact test was performed in R statistical software (http://www.r-project.org/).

Detecting Initiation of ON Periods. ON periods were detected by binning spikes from all units in 50-ms time bins and then setting a threshold to detect local peaks in the spike rate. The threshold was determined manually for each patient after visually checking to ensure adequate detection, because the number of units and thus expected population spike rates differed in each patient. After detection, the first spike within 300 ms of ON period detection was taken as the initiation time, and spike histograms verified that these times represented initiation of spiking. These ON period initiation times then were used for subsequent analysis of slow oscillation spectra and waveform morphology.

ACKNOWLEDGMENTS. We thank A. Dykstra and A. Chan for help with electrode localization methods, A. Smith for sharing spike rate Bayesian estimation code, and D. Ba for assistance with GLM fitting code. This work was funded by a grant from the Center for Integration of Medicine and Innovative Technology and by National Institutes of Health (NIH)/National Institute of Neurological Disorders and Stroke (NINDS) Grants NS062092 (to S.S.C.) and K08NS066099-01A1 (to W.S.A.); by National Eye Institute Grant EY017658, National Institute on Drug Abuse Grant NS063249, National Science Foundation Grant IOB 0645886, the Howard Hughes Medical Institute, and the Klingenstein Foundation (to E.N.E.); by NIH Director's Pioneer Award DP1OD003646 and Grant R01-MH071847 (to E.N.B.); by a Department of Veterans Affairs Career Development Transition Award, a Doris Duke Charitable Foundation–Clinical Scientist Development Award, Massachusetts General Hospital–Deane Institute for Integrated Research on Atrial Fibrillation and Stroke, and NIH/National Institute on Deafness and Other Communications Disorders Grant R01DC009899 (to L.R.H.); by a Canadian Institute of Health Research Fellowship (to L.D.L.); and by NIH New Innovator Award DP2-OD006454 and K-Award K25-NS057580 (to P.L.P.).

1. Brown EN, Lydic R, Schiff ND (2010) General anesthesia, sleep, and coma. *N Engl J Med* 363(27):2638–2650.
2. Rudolph U, Antkowiak B (2004) Molecular and neuronal substrates for general anaesthetics. *Nat Rev Neurosci* 5(9):709–720.
3. Bai D, Pennefather PS, MacDonald JF, Orser BA (1999) The general anesthetic propofol slows deactivation and desensitization of GABA(A) receptors. *J Neurosci* 19 (24):10635–10646.
4. Brown EN, Purdon PL, Van Dort CJ (2011) General anesthesia and altered states of arousal: A systems neuroscience analysis. *Annu Rev Neurosci* 34:601–628.
5. Alkire MT, et al. (1995) Cerebral metabolism during propofol anesthesia in humans studied with positron emission tomography. *Anesthesiology* 82(2):393–403, discussion 27A.
6. Fiset P, et al. (1999) Brain mechanisms of propofol-induced loss of consciousness in humans: A positron emission tomographic study. *J Neurosci* 19(13):5506–5513.
7. Kungys G, Kim J, Jinks SL, Atherley RJ, Antognini JF (2009) Propofol produces immobility via action in the ventral horn of the spinal cord by a GABAergic mechanism. *Anesth Analg* 108(5):1531–1537.
8. Steriade M, Nuñez A, Amzica F (1993) A novel slow (< 1 Hz) oscillation of neocortical neurons in vivo: Depolarizing and hyperpolarizing components. *J Neurosci* 13(8): 3252–3265.
9. Murphy M, et al. (2011) Propofol anesthesia and sleep: A high-density EEG study. *Sleep* 34(3):283–91A.
10. Feshchenko VA, Veselis RA, Reinsel RA (2004) Propofol-induced alpha rhythm. *Neuropsychobiology* 50(3):257–266.
11. Supp GG, Siegel M, Hipp JF, Engel AK (2011) Cortical hypersynchrony predicts breakdown of sensory processing during loss of consciousness. *Curr Biol* 21(23): 1988–1993.
12. Cimenser A, et al. (2011) Tracking brain states under general anesthesia by using global coherence analysis. *Proc Natl Acad Sci USA* 108(21):8832–8837.
13. Akrawi WP, Drummond JC, Kalkman CJ, Patel PM (1996) A comparison of the electrophysiologic characteristics of EEG burst-suppression as produced by isoflurane, thiopental, etomidate, and propofol. *J Neurosurg Anesthesiol* 8(1):40–46.
14. Ching S, Purdon PL, Vijayan S, Kopell NJ, Brown EN (2012) A neurophysiological–metabolic model for burst suppression. *Proc Natl Acad Sci USA* 8(109):3095–3100.
15. Contreras D, Steriade M (1995) Cellular basis of EEG slow rhythms: A study of dynamic corticothalamic relationships. *J Neurosci* 15(1 Pt 2):604–622.
16. Bennett C, Voss LJ, Barnard JP, Sleigh JW (2009) Practical use of the raw electroencephalogram waveform during general anesthesia: The art and science. *Anesth Analg* 109(2):539–550.
17. Mashour GA (2004) Consciousness unbound: Toward a paradigm of general anesthesia. *Anesthesiology* 100(2):428–433.
18. Alkire MT, Hudetz AG, Tononi G (2008) Consciousness and anesthesia. *Science* 322 (5903):876–880.
19. Truccolo W, et al. (2011) Single-neuron dynamics in human focal epilepsy. *Nat Neurosci* 14(5):635–641.
20. Steriade M, Contreras D, Curró Dossi R, Nuñez A (1993) The slow (< 1 Hz) oscillation in reticular thalamic and thalamocortical neurons: Scenario of sleep rhythm generation in interacting thalamic and neocortical networks. *J Neurosci* 13(8):3284–3299.
21. Nir Y, et al. (2011) Regional slow waves and spindles in human sleep. *Neuron* 70(1): 153–169.
22. Vyazovskiy VV, et al. (2009) Cortical firing and sleep homeostasis. *Neuron* 63(6): 865–878.
23. Lachaux JP, Rodriguez E, Martinerie J, Varela FJ (1999) Measuring phase synchrony in brain signals. *Hum Brain Mapp* 8(4):194–208.
24. Breshears JD, et al. (2010) Stable and dynamic cortical electrophysiology of induction and emergence with propofol anesthesia. *Proc Natl Acad Sci USA* 107 (49):21170–21175.
25. Vincent JL, et al. (2007) Intrinsic functional architecture in the anaesthetized monkey brain. *Nature* 447(7140):83–86.
26. Truccolo W, Eden UT, Fellows MR, Donoghue JP, Brown EN (2005) A point process framework for relating neural spiking activity to spiking history, neural ensemble, and extrinsic covariate effects. *J Neurophysiol* 93(2):1074–1089.
27. Schwarz G (1978) Estimating the dimension of a model. *Annals of Statistics* 6(2): 461–464.
28. Timofeev I, Grenier F, Bazhenov M, Sejnowski TJ, Steriade M (2000) Origin of slow cortical oscillations in deafferented cortical slabs. *Cereb Cortex* 10(12):1185–1199.
29. Sanchez-Vives MV, McCormick DA (2000) Cellular and network mechanisms of rhythmic recurrent activity in neocortex. *Nat Neurosci* 3(10):1027–1034.
30. Blethyn KL, Hughes SW, Tóth TI, Cope DW, Crunelli V (2006) Neuronal basis of the slow (<1 Hz) oscillation in neurons of the nucleus reticularis thalami in vitro. *J Neurosci* 26(9):2474–2486.
31. Crunelli V, Hughes SW (2010) The slow (<1 Hz) rhythm of non-REM sleep: A dialogue between three cardinal oscillators. *Nat Neurosci* 13(1):9–17.
32. John ER, et al. (2001) Invariant reversible QEEG effects of anesthetics. *Conscious Cogn* 10(2):165–183.
33. Timofeev I, Grenier F, Steriade M (2001) Disfacilitation and active inhibition in the neocortex during the natural sleep-wake cycle: An intracellular study. *Proc Natl Acad Sci USA* 98(4):1924–1929.
34. Amzica F, Steriade M (1995) Short- and long-range neuronal synchronization of the slow (< 1 Hz) cortical oscillation. *J Neurophysiol* 73(1):20–38.
35. Destexhe A, Hughes SW, Rudolph M, Crunelli V (2007) Are corticothalamic 'up' states fragments of wakefulness? *Trends Neurosci* 30(7):334–342.
36. Ogilvie RD (2001) The process of falling asleep. *Sleep Med Rev* 5(3):247–270.
37. Achermann P, Borbély AA (1997) Low-frequency (< 1 Hz) oscillations in the human sleep electroencephalogram. *Neuroscience* 81(1):213–222.
38. Cash SS, et al. (2009) The human K-complex represents an isolated cortical down-state. *Science* 324(5930):1084–1087.
39. Bersagliere A, Achermann P (2010) Slow oscillations in human non-rapid eye movement sleep electroencephalogram: Effects of increased sleep pressure. *J Sleep Res* 19(1 Pt 2):228–237.
40. Csercsa R, et al. (2010) Laminar analysis of slow wave activity in humans. *Brain* 133(9): 2814–2829.
41. Chauvette S, Crochet S, Volgushev M, Timofeev I (2011) Properties of slow oscillation during slow-wave sleep and anesthesia in cats. *J Neurosci* 31(42):14998–15008.
42. Vyazovskiy VV, et al. (2011) Local sleep in awake rats. *Nature* 472(7344):443–447.
43. Ching S, Cimenser A, Purdon PL, Brown EN, Kopell NJ (2010) Thalamocortical model for a propofol-induced alpha-rhythm associated with loss of consciousness. *Proc Natl Acad Sci USA* 107(52):22665–22670.
44. Young GB (2000) The EEG in coma. *J Clin Neurophysiol* 17(5):473–485.
45. Blumenfeld H, et al. (2004) Ictal neocortical slowing in temporal lobe epilepsy. *Neurology* 63(6):1015–1021.
46. Lewicki MS (1998) A review of methods for spike sorting: The detection and classification of neural action potentials. *Network* 9(4):R53–R78.
47. Smith AC, et al. (2010) State-space algorithms for estimating spike rate functions. *Comput Intell Neurosci*, 10.1155/2010/426539.
48. Tort ABL, Komorowski R, Eichenbaum H, Kopell N (2010) Measuring phase-amplitude coupling between neuronal oscillations of different frequencies. *J Neurophysiol* 104 (2):1195–1210.
49. Dykstra AR, et al. (2012) Individualized localization and cortical surface-based registration of intracranial electrodes. *Neuroimage* 59:3563–3570.
50. Komarek P (2005) *Making Logistic Regression a Core Data Mining Tool* (Robotics Institute).
51. Brillinger D (1976) Estimation of the second-order intensities of a bivariate stationary point process. *Journal of the Royal Statistical Society. Series B (Methodological)* 38(1): 60–66.